WELDING RESEARCH

SUPPLEMENT TO THE *WELDING JOURNAL*, DECEMBER 1987

Sponsored by the American Welding Society and the Welding Research Council

Experimental Measurement of Thin Plate 304 Stainless Steel GTA Weld Pool Surface Temperatures

The possibility of regional undercooling caused by constitutional supercooling was investigated

BY H. G. KRAUS

ABSTRACT. The optical spectral radiometric/laser reflectance method was used to noninvasively measure arc-side GTA weld pool surface temperatures for 1.5-mm-thick (0.05-in.) stainless steel plate Type 304. High-resolution weld pool surface temperature isothermal contour and topology plots, as well as lengthwise centerline temperature profiles, were generated for welding currents of 38, 50 and 70 A; welding voltages of 7.5, 8.0 and 8.5 V, respectively; and welding speeds of 0.423, 1.270 and 2.540 mm/s (1, 3 and 6 ipm), respectively. The primary purpose of the work was to investigate the possibility of regional undercooling or supercooling, caused by constitutional supercooling, via weld pool surface temperature measurements, in the tail region of the weld pools. Although it is well known that constitutional supercooling can be present in alloy solidification, no resulting measurable undercooling was detected. Results showed peak weld pool temperatures in the range of 2000 to 2800 K and were often found to lead the electrode instead of lag behind it, as might be intuitively expected. A qualitative explanation for the latter is provided. These results were compared to those for spot temperature experimental measurements of electron beam welds and other stainless steel Type 304 GTA welds, as well as predictions based on vaporization theory. Additionally, it was found that, under most conditions, no two weld pools are alike and that the concept of quasi-steady-state pools does not represent reality. They are instead dynamically (stochastically) varying about mean value representative characteristics.

KEY WORDS

Experimental Measures
Thin Plate SS 304
GTA Weld Pools
Surface Temperature
Emissive Power
Laser Reflectance
SS 304 Emissivity
Weld Pool Tail
Nucleation
Supercooling

H. G. KRAUS is a Senior Engineer Specialist with Idaho National Engineering Laboratory, EG&G Idaho, Inc., Idaho Falls, Idaho.

Paper presented at the AWS 68th Annual Meeting, held March 22-27, 1987, in Chicago, Ill.

Introduction

The measurement of weld pool surface temperatures is important to welding science and technology for several reasons. These include verifying theoretical model predictions of the thermal physics of the weld pool and of the plasma physics of the welding arc. Such information was used here to investigate the possibility of undercooling caused by constitutional supercooling in the tail region of GTA weld pools. Past GTA theoretical weld pool modeling of thin plate Type 304 revealed an increasing shape discrepancy (with no discrepancy in the overall area), relative to experimental measurements, in the weld pool tail region as the welding power and velocity were increased (Ref. 1). Predicting the

correct shape in the pool tail region is important because crystal growth associated with constitutional supercooling occurs within 30 to 40 deg of normal to the phase front, and thus directly affects microstructure formation (Ref. 2). The microstructure information is in turn useful for the prediction of macrostructural properties throughout the weld. Two possible mechanisms for explaining the above discrepancy were identified: arc heat flux drag due to arc/anode electromagnetic field interaction, and constitutionally induced supercooling or undercooling. Only the latter was investigated here.

Solidification, as well as melting, of metals occurs by nucleation and growth. Solid phase nucleation during freezing is a much more difficult process than the formation of nuclei in the liquid phase during melting (Ref. 3). Thus, metals do not superheat to any appreciable extent when they are liquified, whereas some supercooling occurs nearly every time a metal is solidified. If conditions during solidification permit homogeneous nucleation, liquid metals can be cooled far below their equilibrium freezing points before solidification begins. For example, supercooling of 130, 319 and 295 K have been achieved under rigidly controlled experimental conditions for aluminum, nickel and iron, respectively (Ref. 3). Crystal nuclei formation during solidification is related to the positive interfacial energy of the solid-liquid phase boundary. The volume free-energy decrease that is associated with the formation of the solid phase is opposed by the free energy of the surface that is created when the nucleus is formed. A critical nuclei size exists that must be exceeded for newly formed crystals to grow. As the temperature drops below the equilibrium freezing temperature, the volume free-energy term increases more rapidly than the surface free energy, causing a decrease in critical nucleus size with the increased supercooling, until, at the homogeneous nucleation temperature, the critical nucleus size becomes small enough that stable nuclei can form as a result of the thermal fluctuations of the atoms. As the nuclei form, the heat of fusion tends to counteract the supercooling and the temperature of the melt rises toward the equilibrium freezing point.

The extent to which supercooling may be occurring in the tail region of the above Type 304 GTA welds was investigated here. Kraus (Ref. 1) showed that a weld pool tail region supercooling of 140 K would be sufficient to explain the aforementioned experimental/model discrepancy for the maximum welding current, 70 A, and maximum welding speed, 2.54 mm/s (1 ipm) used. Neither equilibrium nor homogeneous solidification conditions are expected in welding processes, but rather conditions between the two extremes. The 140 K supercooling was seen as feasible since it lies between the 0 K equilibrium solidification and the ~300 K homogeneous nucleation solidification of iron or nickel (constituents of 304) mentioned above.

Easterling (Ref. 4) has discussed in detail metal alloy solidification processes and has shown qualitatively that specific cooling scenarios of the weld material can indeed result in a phenomenon known as constitutional supercooling. Easterling provides the following explanatory scenario for weld pool alloy solidification. Because of turbulence and convection in the liquid beneath the arc, alloy solute redistribution occurs efficiently. As the heat source moves away from a given region and solidification advances, mixing of the solute gives way to diffusional processes. Specific cooling scenarios, resulting in cellular-dendritic growth, lead to the onset of constitutional supercooling. These scenarios were seen to be associated with higher welding speeds. Easterling also provided an explanation of the effect of welding speed on crystal growth and orientation during solidification. It was shown that increasing welding speeds results in elongated, pointed weld pool tails. Subsequent experimental and theoretical investigations by Kraus (Ref. 1) strongly supported the idea that elongated weld pool tails and constitutional supercooling are closely associated. The goal of this research was to search for weld pool surface temperature based evidence of tail region undercooling caused by constitutional supercooling that is induced by higher welding velocities, and to provide the temperature information necessary to check the theoretical thermal models.

Review of Temperature Measurement Methods

Before this decade, weld pool and the surrounding heat-affected zone (HAZ) workpiece temperatures were measured using thermocouples. This results in errors due to thermal loading caused by the presence of the wire and by pool circulation impediment, as well as producing temperature measurements at only a few locations. Weld pool surface temperatures have not been, and for these reasons cannot be, measured using thermocouples.

The only known weld pool surface temperature measurements are those by Shauer, *et al.* (Ref. 5), for electron beam welds, and Giedt, *et al.* (Ref. 6), for GTA welds. In both cases, the method used was narrow band infrared pyrometry. However, the emissivities of the molten metal surfaces were measured only at the liquid-to-solid phase change temperature, and the associated angle was unspecified. Thus, the dependence of emissivity on angle and temperature was unknown. The wavelength of these measurements was specified to be 1.4 μm and 1.526 μm, respectively. Low resolution, 0.5-mm spot size, temperature measurements were made along the centerline lengthwise axis of aluminum and steel alloys, and of tantalum by Shauer, *et al.*, whereas a 1.0-mm spot size was used by Giedt, *et al.*, for the 303 S and 304 stainless steel measurements. It does not appear as though angular dependencies were addressed in these works.

In related research, Sampson, *et al.* (Ref. 7), Chin, *et al.* (Ref. 8), Khan, *et al.* (Ref. 9), and Lukens and Morris (Ref. 10) have investigated the use of infrared thermographic cameras for welding control. Adaptive welding, using fiber optic thermographic sensing, has been developed by Boillot, *et al.* (Ref. 11). However, weld pool surface measurements in these works were of relative emissive power and not of temperature. Lukens and Morris correlated their infrared emission intensity measurements to temperature, using embedded thermocouple data. These thermocouples were buried an average of 2 mm (0.08 in.) below the weld pool surface. Aside from the thermal loading mentioned above, the correlation of the thermocouple data to actual weld pool surface temperatures was unknown.

Other possible methods of weld pool surface temperature measurements are two-color pyrometry (Ref. 12), which assumes that emissivity is independent of wavelength, and four-wavelength pyrometry (Ref. 13), which has been used to simultaneously measure emissivity and temperature in high-reflected flux regions of solar energy collectors for nongray surfaces, with no assumptions regarding emissivity. The experimental weld pool surface temperature measurement method used here, optical spectral radiometric/laser reflectance (Refs. 14,15), also requires no assumptions with respect to the dependence of emissivity on temperature, direction or wavelength, and in fact, permits measurement of such.

Weld Pool Surface Temperature Measurement Method

The details of the experimental measurement of weld pool surface temperatures using the optical spectral radiometric/laser reflectance technique have been given by Kraus (Refs. 14,15). The equation derived there for determining absolute surface temperature is:

$$T = \frac{C_2}{\lambda \ln\left[1 + \frac{(2C_1 \cos\beta)\,\epsilon'_\lambda(\lambda,\beta,T)}{\lambda^5 e'_\lambda(\lambda,\beta,T)}\right]} \quad (1)$$

Table 1—AISI 304 Stainless Steel Composition Analysis Results

Element	Atomic Weight Percent
C	0.1
Cr	17.52
Fe	72.15
Mn	1.6
Mo	0.28
Ni	7.75
P	0.039
S	0.015
Si	0.5
V	0.051

Table 2—Conditions Summary of the 304 Stainless Steel Thin Plate GTA Weld Pool Surface Temperature Measurement Runs and the Maximum Temperature Results[a]

Case	Voltage, V	Current, A	Welding Speed, mm/s (ipm)	Time after Beginning of Emissions Decay, ms	Maximum Temperature, K (°C)	Ratio of Welding Power to Welding Speed, W/(mm/s)
1	8.00	38	0.423 (1)	28.6 ± 3.6	2802 ± 50 (2529)	718.7
2	8.25	50	1.270 (3)	25.0 ± 3.6	2026 ± 40 (1753)	324.8
3	8.25	50	1.270 (3)	25.0 ± 3.6	2119 ± 40 (1846)	324.8
4	8.25	70	2.540 (6)	28.6 ± 3.6	2098 ± 40 (1825)	227.4
5	8.50	70	2.540 (6)	28.6 ± 3.6	2278 ± 40 (2003)	234.3

(a) Ambient or beginning plate temperatures were 291 K (18°C).

which is based on Planck's blackbody spectral distribution of emissive power, the definition of spectral directional emissivity, and Lambert's cosine law of diffuse emitters (see Ref. 16 for definitions). In Equation 1, ϵ'_λ is the spectral directional emissivity, e'_λ is the spectral directional emissive power, λ is wavelength, β is the angle from the normal vector to a surface, and C_1 and C_2 are constants (Ref. 16). To determine absolute temperature, this method requires measurement of ϵ'_λ and e'_λ across the weld pool. The spectral directional emissive power was determined by using high-speed cinematography to photograph the weld pool emissions through a narrow laserline interference filter with its peak transmission at 632.8 nm, as the welding arc was extinguished, so as to have a spectral image of the weld pool immediately after the arc emissions cease. Filming speed was a critical parameter in obtaining useful information with respect to film image density. Controlled processing was used to develop the film, as well as spectral sensitometry (using the laserline filter), to calibrate the film for recorded density as a function of exposure. The film images were microdigitized for density using a 60 μm square pixel, thus producing high-resolution data. Noise in the images, caused by grain clumping, was filtered out using a digital convolution filter. Calibration of film density was performed by matching the actual weld pool size to a particular film image density contour at the phase front of the weld pool where the temperature is known. This temperature was assumed to be the average of the liquidus and solidus temperatures for the alloy. Density values at all digitized pixel locations were then converted to emissive power values, via the sensitometry data. The spectral directional reflectivity of the weld pool was measured as a function of location, and thus temperature, by reflecting a focused helium-neon laser beam, operating at 632.8 nm, off of the weld pool. This in turn enabled the spectral directional emissivity of the weld pool to be determined. It was found that $\epsilon'_\lambda = 0.41 \pm 0.01$ over a broad range from near melting, 1700 K, to over 2600 K. Emissive power and emissivity data, measured at a common angle of $\beta = 48$ deg and a common wavelength of 632.8 nm, were then used simultaneously, at any given film image pixel location, to determine the absolute temperature of the weld pool. Computer routines were written to generate detailed temperature contour and temperature topology plots of the weld pools.

Weld Pool Surface Temperature Results and Discussion

All the welds reported here were made with a Miller Syncrowave 300 welding machine and a 3.2-mm (⅛-in.), 30-deg cone angle, tungsten electrode, with 8.5 L/min (18 cfph) argon cover gas flow. A compositional analysis of the 1.5-mm-thick stainless steel plate Type 304 used is given in Table 1. The welding parameter conditions for which weld pool surface absolute temperatures were measured for GTA welds on 304 plates are summarized in Table 2. Also listed there are the maximum temperatures observed in the weld pools for each case, and the time interval of arc emissions decay. The temperatures of Table 2 are those which occur immediately after arc emissions cease. In the region of arc impingement on the weld pool surface, temperatures presumably have dropped a small amount during the 25 to 30 ms of emissions decay. The arc breaks contact with the pool at ~15 ms into emissions decay, at which time the energy input to the pool, via the arc, ends. Obscuring plasma emissions continue for another 10 to 15 ms. However, moving away from the plasma region of the arc, weld pool temperatures were not seen to change measurably, and the molten region of the weld pool does not change shape or size during arc decay. It takes 1300 to 1500 ms for these weld pools to solidify. Since this research was performed, it has been found that using the emergency shutoff on an Astro Arc Astromatic E-300-PC welding unit decreases the arc emissions decay period by an order of magnitude, *i.e.*, to 2 to 3 ms under the welding conditions used here. This is due to the presence of a large transistor diversion bank to which the inductively stored energy of the welding machine can be rapidly diverted. The Miller welding machine has no such diversion bank. The period of arc emissions decay is a function of welding current when using the Astro Arc and will be reported in detail in a future article. Future research will also repeat the measurements of this article, using the Astro Arc to assess the effect on peak temperatures in Table 2.

Figures 1 through 5 show the weld pool surface temperature contours in intervals of 50 K for the cases of Table 2, respectively. Only temperatures equal to or above the phase change temperature of 1700 K are shown. Evident in these plots are the electrode, its spectral reflection in the weld pool, and its diffuse reflection off of the solid phase metal. The electrode and its reflection temperatures are fictitious because its emissivity was not measured. Because the electrode absolute temperatures were not of interest, the molten stainless steel 304 emissivity was used in these regions. (Future work will include writing a computer algorithm to subtract the electrode and its reflection and perform temperature fill-in of these regions.) Figures 6 through 10 are the temperature topology plots corresponding to Figs. 1 through 5, for which the above comments also apply. The lengthwise centerline weld pool temperature profiles are also presented in Figs. 11 through 13, where the results from the two 50-A runs have been superimposed, as have also the results from the two 70-A runs. It is evident from these plots that weld pool surface temperature profiles vary in nature very much like human fingerprints—no two are the same. Table 2 data include the estimated error bands for the maximum temperatures observed, calculated as per the example given by Kraus (Ref. 15). Note that the maximum temperatures are known to within 40 to 50 K. However, in the tail region and near the phase front of

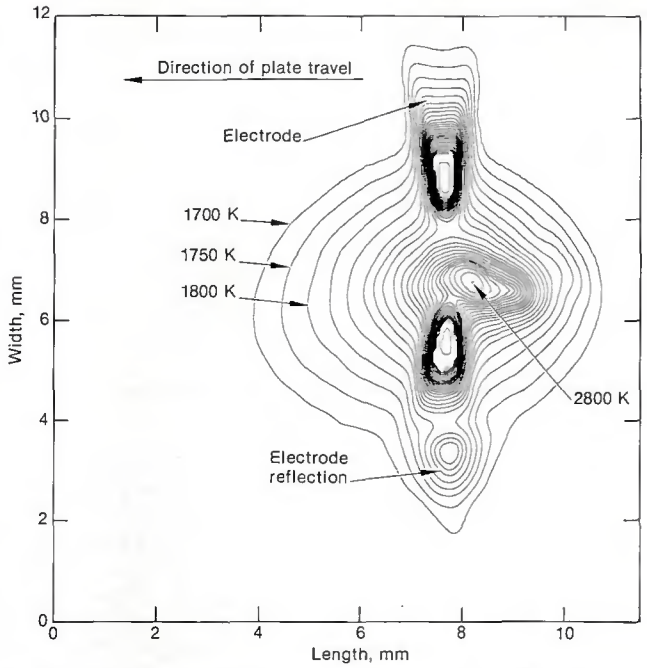

Fig. 1—Weld pool surface isothermal temperature contours for 304 stainless steel, 8 V, 38 A, 0.423 mm/s. (Case 1 of Table 2)

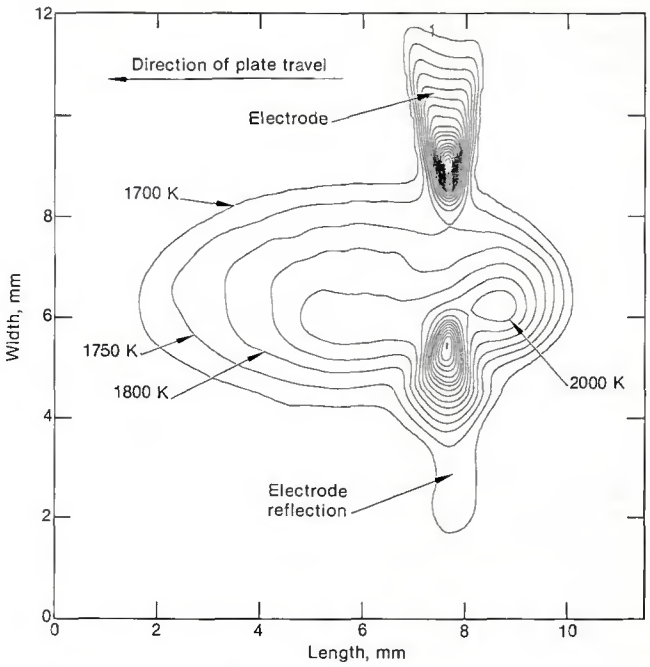

Fig. 2—Weld pool surface isothermal temperature contours for 304 stainless steel, 8.25 V, 50 A, 1.27 mm/s. (Case 2 of Table 2)

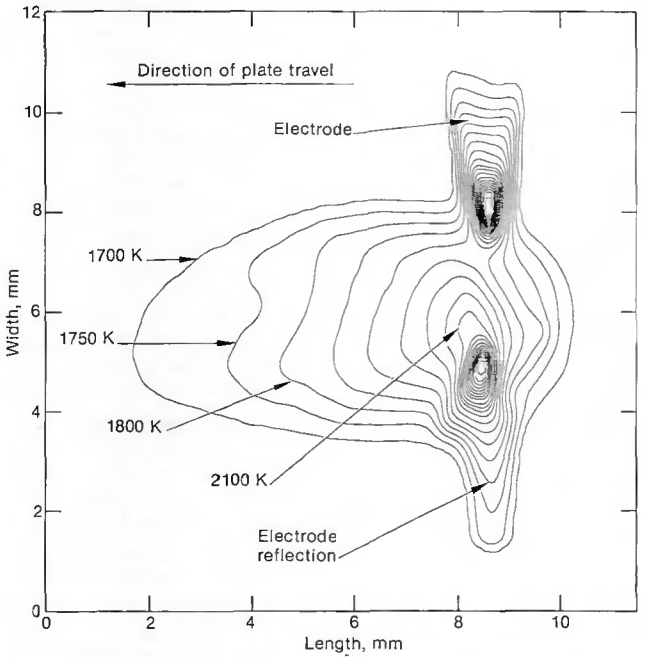

Fig. 3—Weld pool surface isothermal temperature contours for 304 stainless steel, 8.25 V, 50 A, 1.27 mm/s. (Case 3 of Table 2)

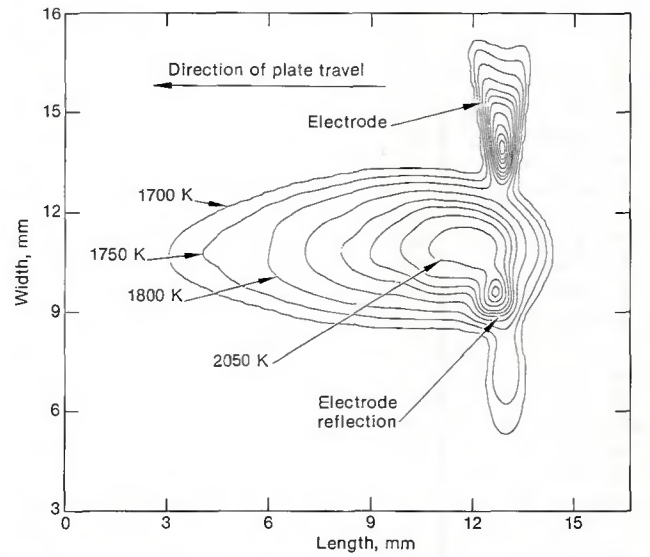

Fig. 4—Weld pool surface isothermal temperature contours for 304 stainless steel, 8.25 V, 70 A, 2.54 mm/s. (Case 4 of Table 2)

the weld pool, the absolute error in temperature is less than 30 K. If significant regional supercooling were taking place in the tail regions of the 304 weld pools, temperatures below the 1700 K should have been observed. The second 50-A case shows a double tail effect in the temperature topology of the weld pool, indicating cooler temperatures in the center region than in the regions perpendicularly adjacent to the centerline direction of travel. Recirculation as observed by Kraus (Ref. 1), creating flow in the direction opposite to plate motion (*i.e.*, in the same direction as welding machine motion), may be responsible for this cooler central region. However, within the absolute accuracy of these experimental measurements, no temperatures below 1700 K were found. Constitutional supercooling resulting in an average undercooling magnitude less than 30 K may still be present.

Further examination of the temperature plots of Figs. 1 through 10 shows that the emissive power of the electrode, and, presumably, temperature (if the electrode emissivity is relatively independent of temperature in the high-temperature range expected), is much higher in the 38-A case than the other cases. Since the time of arc emissions decay given in Table 2 appears to be nearly the same in all cases, the explanation for this is probably related to the welding speed and input power and how these affect the weld pool temperatures and energy transport characteristics of the arc and surrounding argon plasma. Additionally,

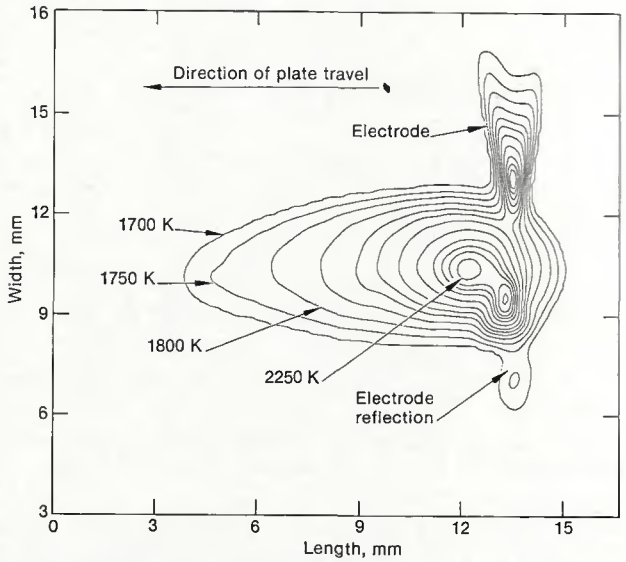

Fig. 5 — Weld pool surface isothermal temperature contours for 304 stainless steel, 8.5 V, 70 A, 2.54 mm/s. (Case 5 of Table 2)

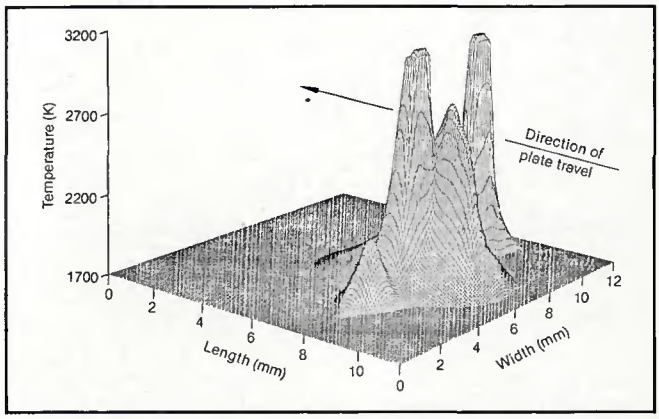

Fig. 6 — Weld pool surface temperature topology plots for 304 stainless steel, 8 V, 38 A, 0.423 mm/s. (Case 1 of Table 2)

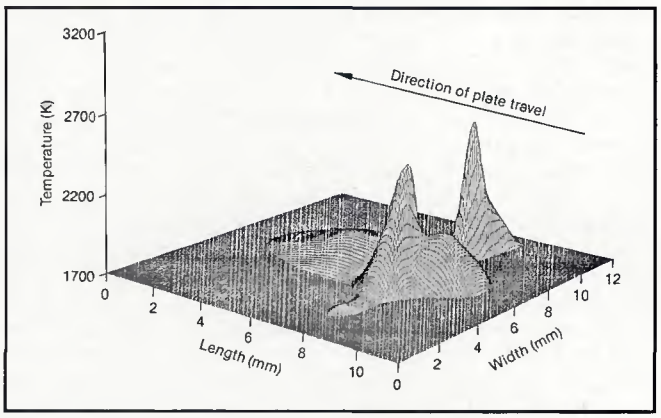

Fig. 7 — Weld pool surface temperature topology plots for 304 stainless steel, 8.25 V, 50 A, 1.27 mm/s. (Case 2 of Table 2)

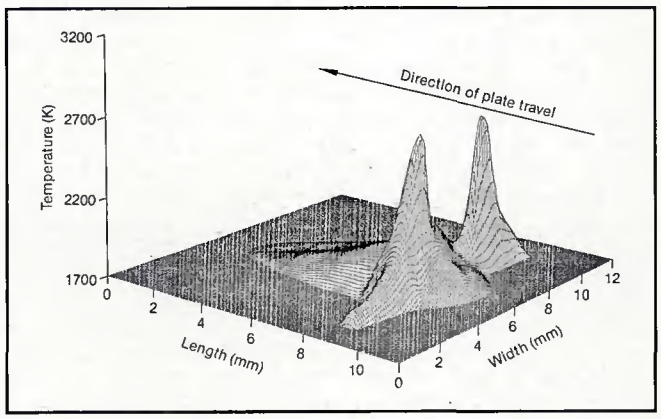

Fig. 8 — Weld pool surface temperature topology plots for 304 stainless steel, 8.25 V, 50 A, 1.27 mm/s. (Case 3 of Table 2)

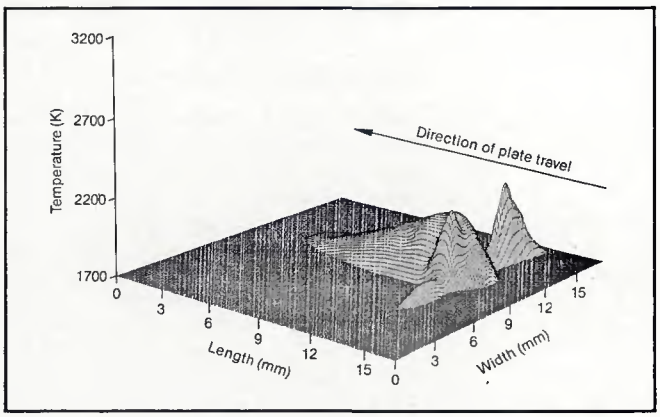

Fig. 9 — Weld pool surface temperature topology plots for 304 stainless steel, 8.25 V, 70 A, 2.54 mm/s. (Case 4 of Table 2)

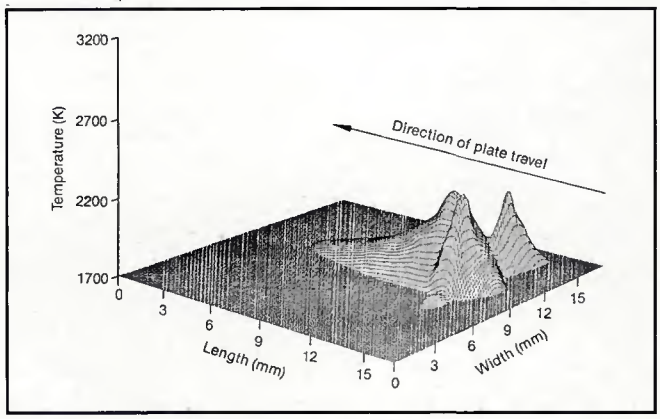

Fig. 10 — Weld pool surface temperature topology plots for 304 stainless steel, 8.5 V, 70 A, 2.54 mm/s. (Case 5 of Table 2)

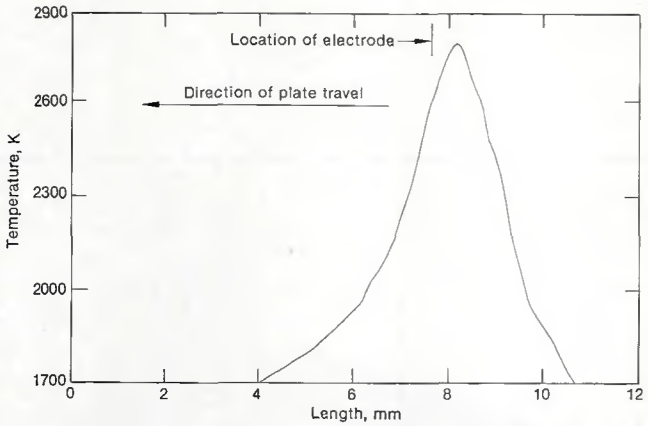

Fig. 11 — Weld pool lengthwise centerline temperature profile for 304 stainless steel, 8 V, 38 A, 0.423 mm/s. (Case 1 of Table 2)

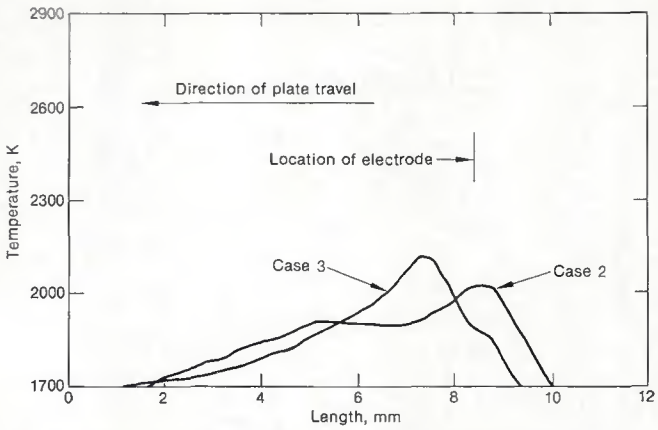

Fig. 12 — Weld pool lengthwise centerline temperature profiles for 304 stainless steel, 8.25 V, 50 A, 1.27 mm/s. (Cases 2 and 3 of Table 2)

since the higher welding currents produce stronger electromagnetic forces, this may induce convective circulation in the weld pool which may affect the concentration of vaporized metal species in the argon plasma. With a high concentration of metallic vapor species in the plasma, an increased plasma electrical conductivity results, which serves to broaden the arc as explained by Johnson and Pfender (Ref. 17). This could influence electrode and weld pool surface temperatures. Details of the physical processes occurring inside the plasma arc are complex and stochastic in nature. They are not well understood, nor predictable within the current technology of welding science.

The maximum temperature results of Table 2 cover a range comparable to: electron beam 304 stainless steel weld pool results of 2100°C (3812°F) with 50°C (90°F) variation between welds by Schauer, *et al.* (Ref. 5); 2000°C (3632°F) peak stationary 304 stainless steel weld pool measurements by Giedt, *et al.* (Ref. 6); and vaporization theory based calculations of 2010°C (3650°F) and 2520°C (4568°F) for 10% and 100%, respectively, of workpiece input energy going into metal vaporization by Block-Bolten and Eagar (Ref. 18). True vaporization energy losses are probably between 1 and 10% (Ref. 18). The higher peak temperature of 2529°C (4584°F) of Case 1, Table 2, can be largely explained by examining the comparative input welding power to welding speed ratio. This ratio is given in the last column of Table 2. Note that this ratio is 2 to 3 times larger for the 38-A (Case 1) run, and thus, the higher maximum temperature of 2529°C, which is essentially at the vaporization limit of 2520°C predicted by Block-Bolten and Eagar, is to be expected. That these maximum temperatures are in such close agreement is evidence to support the idea that weld pool maximum temperatures do not change appreciably during arc emissions decay.

Peak weld pool temperatures for Cases 1 and 2 occur ahead of, instead of behind, the electrode, as expected. In explanation of this phenomenon, it is hypothesized, based on electric potential theory, that the path from the electrode to the weld pool is the one of least potential difference across the gas gap. Videotape observations of the arc impingement point on the weld pool, called the anode spot, show its motion around the weld pool in a somewhat stochastic manner. This is likely due to the fact that the path of minimum potential through the plasma arc is changing due to its unsteady characteristics, even under supposed "quasi-steady-state" conditions. When peak temperatures lie ahead of the electrode, it is likely that the arc impingement point is in this region also, but for obvious reasons, they do not necessarily coincide.

Weld pool cooling rates can easily be determined from the data of Figs. 1 through 5. Different welds made under the same conditions do not necessarily result in the same cooling rates in the tail region of the welds for solidification, as is apparent in Fig. 12. Since the time-averaged solidification rates must be constant during quasi-steady-state welding conditions, this further indicates that the thermal gradients on the surface and in the interior of weld pools must vary considerably about a norm with respect to time, *i.e.,* be very stochastic in nature.

The variability of the weld pool temperatures under quasi-steady-state welding conditions would also have significant implications with respect to the effect of surface tension on weld pool circulation. Since surface tension is temperature dependent for liquid metals, and is proportional to the magnitude of the temperature gradient, surface tension forces could vary dramatically over time, contributing to the variable nature of weld pool temperatures.

Fig. 13 — Weld pool lengthwise centerline temperature profiles for 304 stainless steel, 8.5 V, 70 A, 2.54 mm/s. (Cases 4 and 5 of Table 2)

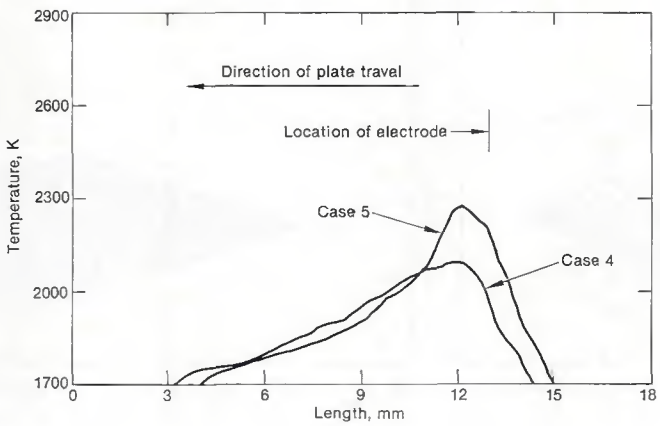

Conclusions

Weld pool surface temperatures have been measured for 304 stainless steel thin plate GTA welds at near quasi-steady-state conditions. The optical spectral radiometric/laser reflectance experimental method was used to make the high-resolution absolute temperature measurements. The possibility of undercooling caused by constitutional supercooling in the tail region of such welds was investigated using these measurements, but was not detected. If significant undercooling due to constitutional supercooling were present, the accuracy of these

measurements would indicate that its magnitude was less than 30 K. The concept of quasi-steady-state conditions under fixed welding current, voltage and speed does not correspond to reality. Rather, the temperature topology of quasi-steady-state weld pools varies considerably, perhaps 5 to 10% in absolute temperature, about a norm with respect to time. Different welds made under the same conditions possess a signature much like human fingerprints—no two are identical.

Acknowledgments

The author gratefully acknowledges the support of the following individuals: Dr. H. B. Smartt for his consistent, enthusiastic support of this research project in his overall welding research program; L. D. Reynolds for his technical assistance and for helping to set up and run the experiments; and J. H. Carson, J. J. Guenette, F. Bunker, R. Liljestrand, and M. A. Lopez of EG&G Measurements, Los Alamos, N. Mex., for their aid in film processing, sensitometry, and image microdigitizing.

This research was funded by the U.S. Department of Energy, Office of Energy Research, Basic Energy Sciences, under contract number DE-AC07-76-ID01570.

References

1. Kraus, H. G. 1986. Thermal finite element formulation and solution versus experimental results for thin-plate GTA welding. *J. Heat Transfer* 108(8):591–596.

2. Slavin, G. A., and Khorosheva, V. G. 1979. Conditions of formation of the structure of weld metal in the welding of thin sheets of creep-resisting materials. *Welding Production* 26(10):5–9.

3. Reed-Hill, R. E. 1966. *Physical Metallurgy Principles,* D. Van Nostrand.

4. Easterling, K. E. 1984. Solidification microstructure of fusion welds. *Mats. Sc. and Eng.* 65:191–198.

5. Schauer, D. A., Giedt, W. H., and Shintaku, S. M. 1978. Electron beam welding cavity temperature distributions in pure metals and alloys. *Welding Journal* 57(5):127-s to 133-s.

6. Giedt, W. H., Wei, X.-C., and Wei, S.-R. 1984. Effect of surface convection on stationary GTA weld zone temperatures. *Welding Journal* 63(12):376-s to 383-s.

7. Sampson, R. E., Suits, G., and Arnold, C. B. March 1985. *Analysis of Sensors for Application of Welding Control.* Report No. 176200-1-F, Environmental Research Institute of Michigan.

8. Chin, B. A., Goodling, J. S., and Madsen, N. H. 1983. Infrared thermography shows promise for sensors in robotic welding. *Robotics Today* 5(1):85–87.

9. Khan, M. A., Madsen, N. H., Goodling, J. S., and Chin, B. A. 1986. Infrared thermography as a control for the welding process. *Opt. Eng.* 25(6):799–805.

10. Lukens, W. E., and Morris, R. A. 1982. Infrared temperature sensing of cooling rates for arc welding control. *Welding Journal* 61(1):27–33.

11. Boillot, J. D., Cielo, P., Begin, G., Michel, C., Lessard, M., Fafard, P., and Villemure, D. 1985. Adaptive welding by fiber optic thermographic sensing: an analysis of thermal and instrumental considerations. *Welding Journal* 64(7):209-s to 217-s.

12. Eckert, E. R. G., and Goldstein, R. J. 1976. *Measurements in Heat Transfer,* 2nd Ed., McGraw-Hill.

13. Zabor, R. S., Lewis, W. S., and Mackie, P. 1984. In situ measurements with a four-wavelength pyrometer. *Heat Transfer,* AICHE Symposium Series, Niagara Falls, N.Y. 80:321–325.

14. Kraus, H. G. 1986. Optical spectral radiometric method for measurement of weld pool surface temperatures. *Optics Letters* 11(12):773–775.

15. Kraus, H. G. To be published. Optical spectral radiometric/laser reflectance method for noninvasive measurement of weld pool surface temperatures. *Opt. Eng.*

16. Siegel, R., and Howell, J. R. 1976. *Thermal Radiation Heat Transfer,* 2nd Ed., McGraw-Hill.

17. Johnson, D. C., and Pfender, E. 1983. The effects of low-ionization potential contaminants on thermal plasmas. *Plasma Chemistry and Plasma Processing* 3(2):259–273.

18. Block-Bolten, A., and Eagar, T. W. 1984. Metal vaporization from weld pools. *Met. Trans. B* 15B(9):461–469.